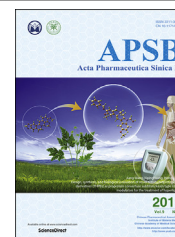




Chinese Pharmaceutical Association
Institute of Materia Medica, Chinese Academy of Medical Sciences

Acta Pharmaceutica Sinica B

www.elsevier.com/locate/apsb
www.sciencedirect.com



ORIGINAL ARTICLE

Novel radioligands for imaging sigma-1 receptor in brain using positron emission tomography (PET)



Yu Lan^{a,d}, Ping Bai^a, Zude Chen^a, Ramesh Neelamegam^b,
Michael S. Placzek^a, Hao Wang^a, Stephanie A. Fiedler^a, Jing Yang^a,
Gengyang Yuan^b, Xiyong Qu^b, Hayden R. Schmidt^c, Jinchun Song^d,
Marc D. Normandin^b, Chongzhao Ran^a, Changning Wang^{a,*}

^aAthinoula A. Martinos Center for Biomedical Imaging, Department of Radiology, Massachusetts General Hospital, Harvard Medical School, Charlestown, MA 02129, USA

^bGordon Center for Medical Imaging, Department of Radiology, Massachusetts General Hospital, Harvard Medical School, Charlestown, MA 02129, USA

^cDepartment of Biological Chemistry and Molecular Pharmacology, Harvard Medical School, Boston, MA 02129, USA

^dDepartment of Pharmacy, Renmin Hospital of Wuhan University, Wuhan 430060, China

Received 6 April 2019; received in revised form 28 June 2019; accepted 4 July 2019

KEY WORDS

σ_1 R;
PET;
Brain imaging;
6-Hydroxypyridazinone;
¹¹C-labeled radioligand

Abstract The sigma-1 receptor (σ_1 R) is a unique intracellular protein. σ_1 R plays a major role in various pathological conditions in the central nervous system (CNS), implicated in several neuropsychiatric disorders. Imaging of σ_1 R in the brain using positron emission tomography (PET) could serve as a noninvasively tool for enhancing the understanding of the disease's pathophysiology. Moreover, σ_1 R PET tracers can be used for target validation and quantification in diagnosis. Herein, we describe the radiosynthesis, *in vivo* PET/CT imaging of novel σ_1 R ¹¹C-labeled radioligands based on 6-hydroxypyridazinone, [¹¹C]HCC0923 and [¹¹C]HCC0929. Two radioligands have high affinities to σ_1 R, with good selectivity. In mice PET/CT imaging, both radioligands showed appropriate kinetics and distributions. Additionally, the specific interactions of two radioligands were reduced by compounds **13** and **15** (self-blocking). Of

Abbreviations: 3D, three-dimensional; σ_1 R, sigma-1 receptor; σ_2 R, sigma-2 receptor; AF, ammonium formate; BBB, brain blood barrier; BP, binding potential; CNS, center nervous systems; CRPS, complex regional pain syndrome; DMF, dimethyl formamide; DMSO, dimethylsulfoxide; ER, endoplasmic reticulum; LCP, lipidic cubic phase; MAM, mitochondria-associated ER membrane; PCP, phencyclidine; PET, positron emission tomography; TFA, trifluoroacetic acid.

*Corresponding author. Tel./fax: +1 617 724 9390.

E-mail address: cwang15@mg.harvard.edu (Changning Wang).

Peer review under responsibility of Institute of Materia Medica, Chinese Academy of Medical Sciences and Chinese Pharmaceutical Association.

<https://doi.org/10.1016/j.apsb.2019.07.002>

2211-3835© 2019 Chinese Pharmaceutical Association and Institute of Materia Medica, Chinese Academy of Medical Sciences. Production and hosting by Elsevier B.V. This is an open access article under the CC BY-NC-ND license (<http://creativecommons.org/licenses/by-nc-nd/4.0/>).

the two, [^{11}C]HCC0929 was further investigated in positive ligands blocking studies, using classic σ_1 R agonist SA 4503 and σ_1 R antagonist PD 144418. Both σ_1 R ligands could extensively decreased the uptake of [^{11}C]HCC0929 in mice brain. Besides, the biodistribution of major brain regions and organs of mice were determined *in vivo*. These studies demonstrated that two radioligands, especially [^{11}C]HCC0929, possessed ideal imaging properties and might be valuable tools for non-invasive quantification of σ_1 R in brain.

© 2019 Chinese Pharmaceutical Association and Institute of Materia Medica, Chinese Academy of Medical Sciences. Production and hosting by Elsevier B.V. This is an open access article under the CC BY-NC-ND license (<http://creativecommons.org/licenses/by-nc-nd/4.0/>).

1. Introduction

As an enigmatic intracellular protein, the history of sigma (σ) receptor was originally categorized as an opioid receptor subtype¹, and later confused with the phencyclidine (PCP) receptor due to the lack of selective ligands². Subsequent pharmacological studies and molecular biology have finally identified that the σ receptor is a non-opioid and non-PCP protein, which was at least two known subtypes, classified as sigma-1 (σ_1) and sigma-2 (σ_2) receptor. These two subtypes are pharmacologically similar but genetically unrelated, with different body distribution, biological function and pharmacological profiles^{3–6}.

At present, sigma-1 receptor (σ_1 R) is known as a unique protein that shares no sequence homology with opioids or any other human proteins but is highly conserved across mammalian species. σ_1 R is a 23.5 kDa that is 223 amino acids in length⁵. σ_1 R is widely expressed in the central nervous system (CNS) and peripheral tissues and organs^{7,8}.

Mainly residing in the mitochondria-associated endoplasmic reticulum (ER) membrane (MAM) of cell, σ_1 R has been reported to interacted with numerous neurotransmitter receptors and ion channels, involved in diverse basic biochemical processes and pathological conditions related to neurodegeneration, pain sensitization, psychiatric disorders, and drug addiction^{7,9,10}. σ_1 R is also found overexpressed in many known human cancers in lung, breast, prostate, and glioma cells^{11,12}.

The first crystal structure of human σ_1 R was recently solved using lipidic cubic phase (LCP) crystallography. The three-dimensional (3D) protein structure of human σ_1 R receptor showed a membrane-bound trimeric assembly with one transmembrane region, modifying the previous hypothesis that the receptor had two transmembrane domains^{13,14}. Despite the fact that structural information has only recently become available, and no endogenous ligand has been established for the receptor, numerous small molecule ligands for σ_1 R have been reported over the past few decades. Among these compounds, some have been developed as radiolabeled imaging tracers (Fig. 1) for positron emission tomography (PET) applications^{15–17}.

As a translational noninvasive imaging method, PET imaging of σ_1 R is a promising modality to evaluate distribution and expression in inaccessible regions and tissues. Additionally, with the specificity and selectivity radioligands, examining σ_1 R through PET could facilitate the investigation of *in vivo* role in pathology and progression of σ_1 R in different diseases directly¹⁸.

Several radiolabeled σ_1 R ligands have been studied in PET imaging of human investigation, but only a few of them have been used clinically. [^{11}C]SA 4503 (**1**) is the first σ_1 R radioligand in human studies¹⁸. The *ex vivo* binding assays of SA 4503 was

initially reported as nanomolar affinity of σ_1 R ($K_i=4.6$ nmol/L) and highly selectivity to σ_1 R ($\sigma_2/\sigma_1=103$)¹⁹, later the selectivity to σ_2 R was reinvestigated as 13.3–55.0^{18,20}. Besides, the low selectivity either to the emopamil binding protein (EBP) or to the vesicular acetylcholine transporter (VACHT) limited its broad use in clinic studies^{19,20}. There are also fluorine-18-labeled σ_1 R radioligands, including but not limited to [^{18}F]FMSA4503²¹ (**2**), [^{18}F]FPS²² (**3**), [^{18}F]SFE^{23,24} (**4**), and [^{18}F]FTC-146²⁵ (**5**). Although most of them have been studied in human researches, and [^{18}F]FTC-146 have completed early phase I trial of PET/MRI in healthy volunteers, and in complex regional pain syndrome (CRPS) and sciatica^{26,27}, still each of them have unmet requirements and needs further investigation for practical clinic translation.

In our previous work, we identified 6-hydroxypyridazinone class of compounds with high σ_1 R affinity and high selectivity over σ_2 R²⁸. *Ex vivo* tests suggested comp-54 (**6**) of 6-hydroxypyridazinone derivatives were reported as the most promising candidate of high binding affinity (σ_1 R $K_i=1.4$ nmol/L) and apparent good selectivity ($\sigma_2/\sigma_1=1365.7$). The pharmacological test of *in vivo* evaluation in rodent showed it was a σ_1 R antagonist and could possibly penetrate the blood–brain barrier (BBB), and get into the σ_1 R-expressed region in mice brain, which exerted a highly potency of modified into σ_1 R radioligand for brain PET imaging. Aiming to preserve this high affinity and selectivity, we devised a strategy to modify **6** in ways that would incorporate a carbon-11 radiolabel without greatly altering the original framework of 6-hydroxypyridazinone in the target molecules.

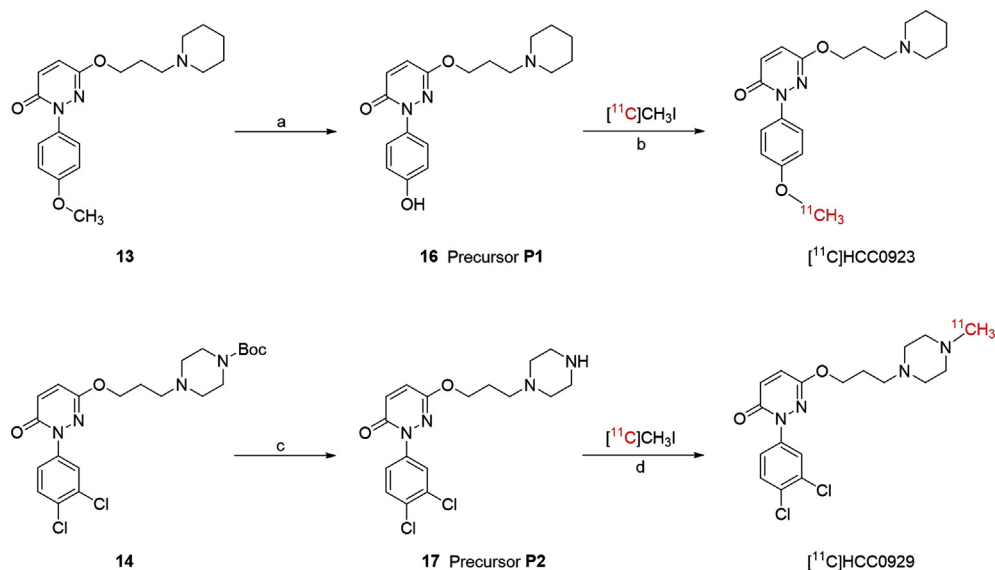
To the best of our knowledge, no similar compounds with 6-hydroxypyridazinone scaffold have been developed as σ_1 R PET radiotracer. Since the core structure is distinct from existing PET radioligands for σ_1 R imaging, it could expand the diversity of available probes and facilitate future advances in a σ_1 R imaging. Here, we report the radiosynthesis of two novel carbon-11-labeled σ_1 R radioligands, [^{11}C]HCC0923 and [^{11}C]HCC0929, and demonstrate the *in vivo* pharmacokinetic properties, biodistribution of brain regions and major organs through PET/CT imaging for σ_1 R in the mice.

2. Results and discussion

2.1. Chemical synthesis

The chemical synthesis of the compounds **13–15** was illustrated in Scheme 1. The 6-hydroxypyridazinone derivatives were prepared following our previously reported work with minor changes^{28,29}.

Briefly, through a one-step cyclization reaction of substitute phenylhydrazine hydrochloride and maleic anhydride, the



Scheme 2 Synthesis of radiolabeling precursor **P1** (16), **P2** (17) and radiosynthesis of [^{11}C]HCC0923 and [^{11}C]HCC0929. Reagents and conditions: (a) BBr_3 , dichloromethane, -78°C to room temperature, overnight; (b) NaOH , DMF, 120°C , 3 min; (c) 2 mol/L HCl in diethyl ether, dichloromethane, room temperature, overnight; (d) K_2CO_3 , DMF, 120°C , 3 min.

The B_{max} of σ_1 R in human brain was measured to be approximately 30–600 fmol/mg (3–60 nmol/L)^{32,33}. Thus, the radioligand with affinity of 0.6–12 nmol/L could be used for σ_1 R imaging, and range of 0.3–6 nmol/L will be more suitable. The *ex vivo* σ_1 R binding affinity of unlabeled HCC0923 (compound **13**) and HCC0929 (compound **15**) were measured through previously demonstrated methods (as described in Supporting Information)^{28,29}. The σ_1 R binding affinities of **13** and **15** were 10.3 and 5.6 nmol/L, with the selectivities of 111.3- and 272.8-fold to σ_2 R, respectively (Table 1^{13,27}). Compared to the most promising compound **6**, both **13** and **15** showed a slight decrease of σ_1 R binding affinity and selectivity, due to structure modifications necessary for radiolabeling; however, based on the criteria mentioned above, **13** and **15** still possessed suitable affinities for *in vivo* PET imaging of σ_1 R.

Besides the binding affinity and selectivity to the target receptor, the $\log D$ is also another important parameter, especially for the radiotracer for brain imaging. The experimental $\log D_{\text{PBS, pH7.4}} \pm \text{SD}$ of compounds **13** and **15** were measured³⁴ to be 0.89 ± 0.06 and 1.73 ± 0.08 , respectively.

2.4. Molecular docking studies of 6-hydroxypyridazinone derivatives

To predict the possible binding mode of the two radioligands, we performed molecular docking with Schrödinger Glide software

Table 1 *Ex vivo* binding affinities for σ_1 R and σ_2 R of PD 144418, compounds **6**, **13** and **15**.

Compd.	σ_1 R K_d or K_i (nmol/L)	σ_2 R K_i (nmol/L)	Selectivity (σ_2 R/ σ_1 R)
PD 144418 ¹³	4.3 ± 0.1	1377 ± 179	—
6 ²⁷	1.4 ± 0.1	1912 ± 210	1365.7
13	10.3 ± 1.1	1146 ± 116	111.3
15	5.6 ± 0.7	1528 ± 120	272.8

—Not applicable.

(Schrödinger, LLC, New York, NY, USA) using the 2.5 Å resolution structure of the σ_1 R bound to PD 144418, in a similar manner as reported previously^{13,14,35}.

Encouragingly, the top-ranked docked pose of PD 144418 in Fig. 2A (yellow) was nearly identical to that seen in the crystal structure (Fig. 2A, cyan), and the Glide score was comparable to

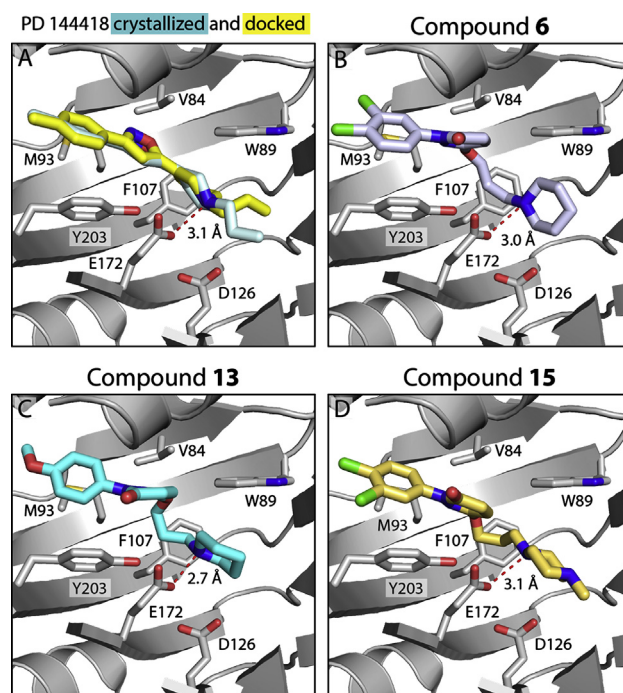


Figure 2 Glide docking of compounds into the σ_1 R (PDB 5HK1). (A) Pose of co-crystallized PD 144418 (pale cyan) and top-ranked pose from Glide docking (yellow). Best docked poses for (B) compound **6** (periwinkle), (C) compound **13** (cyan), (D) compound **15** (gold). In all panels, the receptor is shown in gray.

what has been reported previously for high-affinity σ_1 R ligands^{13,14,35}.

The reference compound **6**, along with **13** and **15**, was docked in the same way. All three compounds adopted similar conformations in the ligand-binding site as PD 144418, with good Glide Scores (Table 2). Like all ligands co-crystallized with the receptor to date, the poses for compounds **6**, **13**, and **15** featured an electrostatic interaction between the positively charged nitrogen in the ligand and E172 (Table 2, Fig. 2B–D). Additionally, as reported for all currently co-crystallized σ_1 R antagonists^{13,14}, the primary hydrophobic regions of these compounds were positioned near Y203, pointing towards the membrane, and the secondary hydrophobic regions were pointing towards the bottom of the ligand binding site past D126. These results suggest that these compounds likely bind the receptor similarly to other high-affinity σ_1 R ligands.

2.5. *In vivo* PET-CT imaging with [¹¹C]HCC0923 in mice^{36,37}

Following the encouraging data in *ex vivo* σ_1 R binding assays and molecular docking, two radioligands, [¹¹C]HCC0923 and [¹¹C]HCC0929, were a step forward to further *in vivo* investigation.

We firstly assessed [¹¹C]HCC0923 *in vivo* conducting dynamic PET imaging focused on mice brains. In PET-CT studies, [¹¹C]HCC0923 exerted high BBB penetration and fast uptake when administered by intravenous bolus injection (100–150 μ Ci per animal), as shown in Fig. 3. Based on a whole-brain analysis, the concentration of [¹¹C]HCC0923 in the mice brain reached a maximum uptake of 6.48% ID/cc within the first few minutes after injection, and sustained binding over the scanning time (60 min).

To investigate the specificity of [¹¹C]HCC0923, we performed PET imaging studies in mice with a 5-min pretreatment of compound **13** (unlabeled HCC0923) at different doses (1.25 and 12.5 mg/kg). Compared with the non-pretreat control (baseline, Fig. 3A), we found that the [¹¹C]HCC0923 binding in mice brain was blocked in a dose-dependent manner with a stepwise reduction in the percent tracer uptake after administration of **13** (Fig. 3B and C). At 1.25 mg/kg, we found an approximate 38% reduction in binding, estimated as the percent change in whole-brain radioactivity between peak uptake at 10 min and the lowest uptake at 60 min. Increasing the dose of **13** to 12.5 mg/kg resulted in a ~54% reduction in [¹¹C]HCC0923 brain uptake, a dose-dependent response to self-blockade and ~45% of uptake attributed to non-specific binding. We observed a similar blockade level at the last 10 min, indicating saturation at 1.25 mg/kg. This finding demonstrates a high specific binding of [¹¹C]HCC0923 for σ_1 R, with a dose-dependent response to self-blockade.

Table 2 Distance of the electrostatic interaction between ligand's basic amine and E172, with Glide scores of PD 144418, HCC0923 and HCC0929 in molecular docking.

Compd.	Distance to E172 (Å)	Glide Score (kcal/mol)
PD 144418 (co-crystallized)	3.1	–
PD 144418 (docking)	3.1	–10.460
6	3.0	–10.251
13	2.7	–10.578
15	3.1	–10.577

–Not applicable.

2.6. *In vivo* PET-CT imaging with [¹¹C]HCC0929 in mice^{36,37}

[¹¹C]HCC0929 was also studied in mice PET-CT imaging due to its better σ_1 R affinity. To test [¹¹C]HCC0929 as a radiotracer *in vivo*, we conducted PET imaging focused on the mice brains. Compared to [¹¹C]HCC0923, we determined that [¹¹C]HCC0929 exhibited more potent properties in PET imaging studies: higher BBB penetration and faster signal decrease over the 60-min scan when administered by intravenous bolus injection (100–150 μ Ci per animal), as shown in Fig. 4.

Unlike the slow gradient of baseline curve of [¹¹C]HCC0923, the whole-brain analysis that exerted the concentration of [¹¹C]HCC0929 in the mice brain reached a maximum uptake of 7.66% ID/cc at ~5 min after injection with moderate wash-out rate during the scanning period (60 min), indicating a faster brain clearance kinetic property compared to [¹¹C]HCC0923. The specificity of [¹¹C]HCC0929 was investigated in mice PET imaging studies with a 5-min i.v. pretreatment of compound **15** (unlabeled HCC0929) at doses of 0.288 and 2.88 mg/kg.

We found that administration of 0.288 mg/kg unlabeled HCC0929 (**15**) blocked [¹¹C]HCC0929 binding in the mice brain by approximately 36%, measured as the percent change in whole radioactivity between peak uptake at ~5 min and the lowest uptake at 60 min. Increasing the dose of **15** to 2.88 mg/kg resulted in a ~58% reduction in [¹¹C]HCC0929 mice brain uptake (Fig. 4D), which represents a dose-dependent response to self-blockade and ~40% of uptake attributed to non-specific binding. The mice *in vivo* PET-CT studies demonstrated a high uptake and good mice brain clearance kinetic of [¹¹C]HCC0929 for σ_1 R imaging in brain, with a dose-dependent response to self-blockade.

2.7. Positive ligands blocking study of *in vivo* PET-CT imaging using [¹¹C]HCC0929 in mice

To further validate the selectivity of σ_1 R of the candidate radioligand [¹¹C]HCC0929, two highly σ_1 R selective ligands, SA 4503 (σ_1 R agonist) and PD 144418 (σ_1 R antagonist) were adopted for positive ligands blocking study^{36,37}.

Through the *in vivo* PET-CT imaging in mice brain (Fig. 5), we found that administration of SA 4503 (2.75 mg/kg) or PD 144418 (2.99 mg/kg) could remarkably reduce the [¹¹C]HCC0929 binding in the mice brain by approximately 41% and 67%, respectively, measured as the percent change in whole radioactivity between peak uptake at ~5 min and the lowest uptake at 60 min. The different blocking effects of two positive ligands might due to their entirely opposite functional profiles. The shape of time–active curve of self-blocking was close to the curve of PD 144418, since the compound **15** acted as the same as antagonist, but the binding affinity to σ_1 R was a little higher than PD 144418.

2.8. *In vivo* biodistribution studies of [¹¹C]HCC0929 in mice

The biodistribution of radioligand [¹¹C]HCC0929 in mice was investigated by *in vivo* PET-CT imaging, and the data were acquired by using the FUSION module in PMOD (PMOD 4.003, PMOD Technologies Ltd., Zurich, Switzerland).

The analysis of detailed distribution of different brain regions of mice was obtained through the mouse (Ma-Benveniste-Mirrione) VOI atlas^{38,39}. Eight important functional regions of mice brain were selected: cortex, cerebellum, brain stem, thalamus,

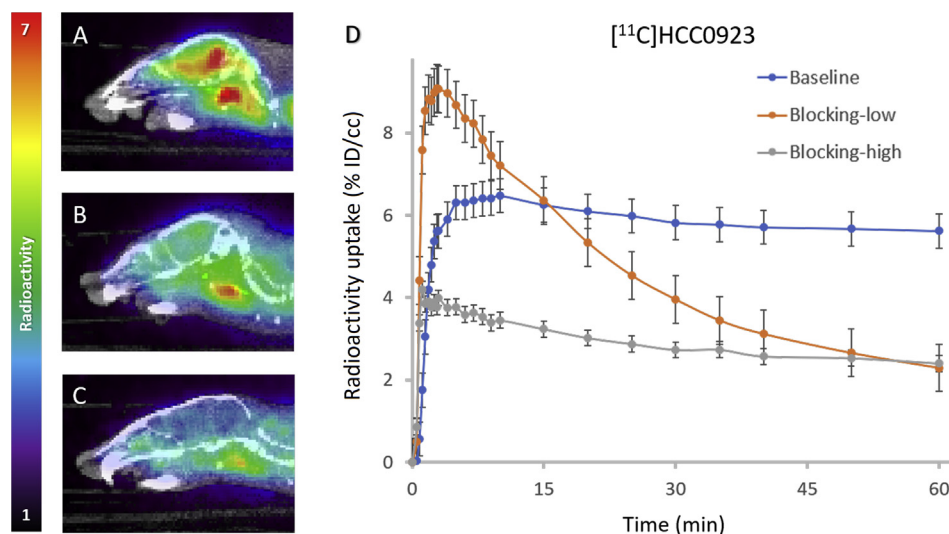


Figure 3 Mice brain PET/CT images 25–60 min after intravenous administration (i.v.) of radioligand [¹¹C]HCC0923 and time–activity curve. (A) Baseline PET/CT image. (B) and (C) PET/CT image from blocking study, involving i.v. pretreatment with unlabeled HCC0923 (self-blocking, B: 1.25 mg/kg, C: 12.5 mg/kg) 5.0 min before radioligand injection. (D) Time–activity curve demonstrating uptake of radioligand for baseline and blocking studies (low & high dose).

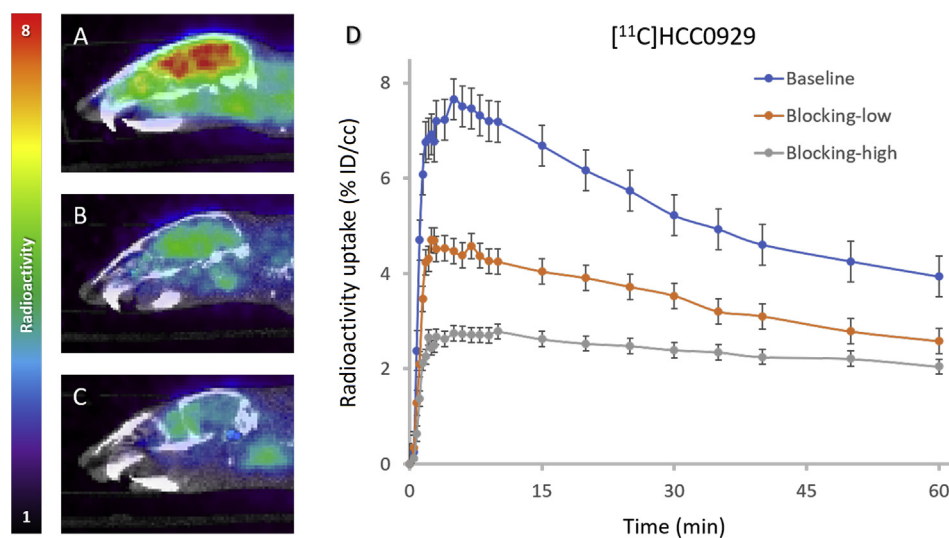


Figure 4 Mice brain PET/CT images 25–60 min after intravenous administration (i.v.) of radioligand [¹¹C]HCC0929 and time–activity curve. (A) Baseline PET/CT image. (B) and (C) PET/CT image from blocking study, involving i.v. pretreatment with unlabeled HCC0929 (self-blocking, B: 0.288 mg/kg, C: 2.88 mg/kg) 5.0 min before radioligand injection. (D) Time–activity curve demonstrating uptake of radioligand for baseline and blocking studies (low & high dose).

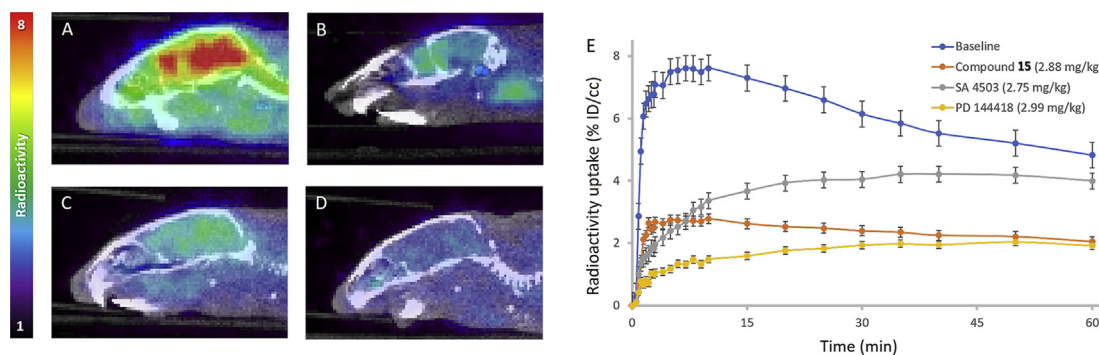


Figure 5 Mice brain PET/CT images 25–60 min after intravenous administration (i.v.) of radioligand [¹¹C]HCC0929 and time–activity curve. (A) Baseline PET/CT image ($n=2$); PET/CT image from blocking study, involving i.v. pretreatment with positive compounds 5.0 min before radioligand injection: (B) unlabeled HCC0929 (self-blocking, 2.88 mg/kg); (C) SA 4503 (σ_1 R agonist, 2.75 mg/kg); (D) PD 144418 (σ_1 R agonist, 2.99 mg/kg); (E) Time–activity curve demonstrating uptake of radioligand for baseline and blocking studies (low & high dose).

hypothalamus, striatum, hippocampus and amygdala. The radioligand [^{11}C]HCC0929 distributed in the selected brain regions were investigated and showed quite similar distribution patterns⁴⁰ without significant regional differences (Fig. 6). In blocking studies, the uptake of [^{11}C]HCC0929 in different regions of mice brain was significantly decreased by co-injection of HCC0929. In high dose injection (2.88 mg/kg), all the selected brain regions of mice were decreased significantly as the same; while pretreated a low dose of HCC0929 (0.288 mg/kg), the cortex, striatum and hippocampus showed a moderate decrease compared to other mice

brain regions, which were mainly because of the different express of $\sigma_1\text{R}$ in these regions.

The distribution of major organs in mice was analyzed using the PBAS module in PMOD 4.003. The mean radioactive uptake in brain and major organs at each time point is showed in Fig. 7. The highest uptake occurred at 5 min in brain ($7.66\pm 0.82\%$ ID/cc), heart ($5.10\pm 0.68\%$ ID/cc), lung ($6.75\pm 0.86\%$ ID/cc) and kidney ($8.87\pm 1.16\%$ ID/cc), and then the radioligand was gradually washed out from these organs. Whereas in liver and spleen, due to the accumulation of [^{11}C]HCC0929, the time point of maximum

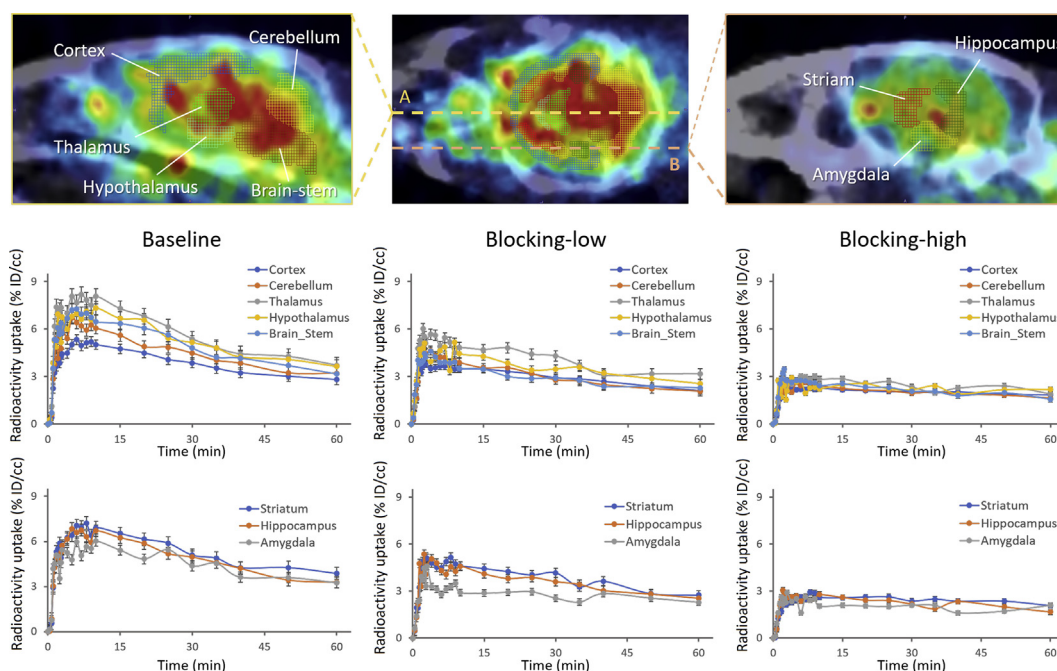


Figure 6 Time-activity curve demonstrating uptake of radioligand [^{11}C]HCC0929 for baseline and blocking studies (self-blocking, low blocking dose: 0.288 mg/kg, high blocking dose: 2.88 mg/kg) of different brain regions of mice brain, including cortex, cerebellum, brain stem, thalamus, hypothalamus, striatum, hippocampus, amygdala.

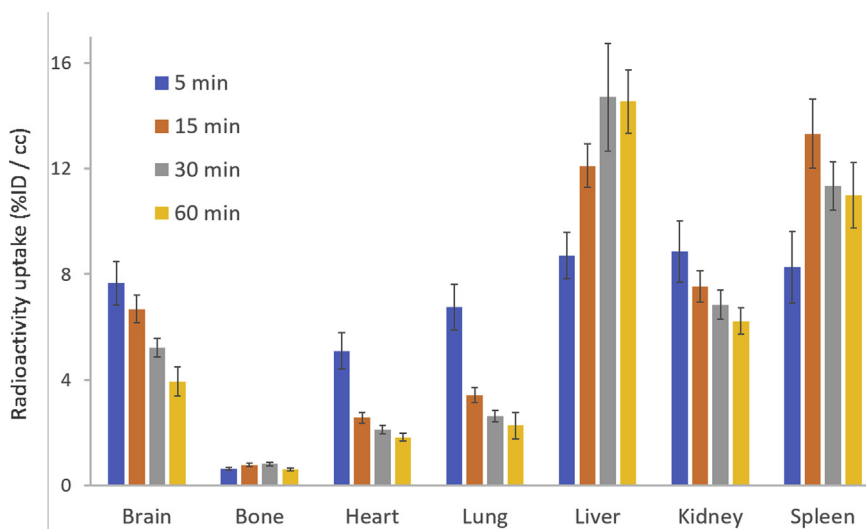


Figure 7 Biodistribution of radioligand [^{11}C]HCC0929 in rats at 5, 15, 30, and 60 min after injection of radioligand ($n=3$ for each time point). Error bars represent SEM.

uptake was behind other organs. The uptake in liver peaked at 30 min at $14.70 \pm 2.03\%$ ID/cc and slightly decreased in 60 min; in spleen, the maximum radioactivity uptake reached in 15 min at $13.32 \pm 2.03\%$ ID/cc and then was slowly washed out during study.

3. Conclusions

In summary, two novel carbon-11 labeled σ_1 R radioligands with a 6-hydroxypyridazinone scaffold, [^{11}C]HCC0923 and [^{11}C]HCC0929, were successfully prepared and evaluated in mice. Both two radioligands can highly bind to σ_1 R in the mice brain, with good selectivity and specificity. Of the two novel ^{11}C -labeled sigma-1 receptor radioligands, [^{11}C]HCC0929 possessed better kinetic property and specificity which was further investigated in positive ligands blocking studies in mice PET-CT brain imaging, using classic σ_1 R agonist SA 4503 and σ_1 R antagonist PD 144418. Both σ_1 R ligands could extensively decrease the uptake of [^{11}C]HCC0929 in mice brain, with different kinetic uptake and washout properties. Besides, the biodistribution of major brain regions and organs of mice were determined *in vivo*. The radioligand [^{11}C]HCC0929 distributed in the selected brain regions showed quite similar distribution patterns as reported, and the distribution in major organs extent the good pharmacokinetic properties *in vivo*. These results demonstrated its promise as preclinical tools for visualizing and quantitating σ_1 R density in the mice brain *in vivo*.

Application [^{11}C]HCC0929 as PET probes could be used to quantify σ_1 R expression in various neurological disorders, and would also be valuable for evaluation of potential drugs in living subjects. The approach is also valuable for expanding the variety and diversity of PET radiotracers for σ_1 R imaging to meet the requirements for practical clinic application and therefore warrants further investigation.

4. Experimental

4.1. General methods and materials

All commercially available chemical reagents and solvents were of ACS-grade purity or higher, and used without further purification.

^1H NMR and ^{13}C NMR spectra data were recorded on a JEOL JNM-ECZ500R Spectrometer (JEOL Ltd, Tokyo, Japan) at 500 MHz (^1H) and 126 MHz (^{13}C) using chloroform-*d*. Chemical shifts were given in δ values (ppm), using tetramethylsilane (TMS) as the internal standard; coupling constants (*J*) were given in Hz. Signal multiplicities were characterized as s (singlet), d (doublet), t (triplet), q (quartet), m (multiplet), and br (broad signal).

Analytical thin layer chromatography (TLC) was performed on silica gel GF254. Column chromatographic purification was carried out using silica gel. Analytical separation was conducted on an Agilent 1100 series HPLC (Agilent Technologies, Inc., Santa Clara, CA, USA) fitted with a diode-array detector, quaternary pump, vacuum degasser, and autosampler. Mass spectrometry data were recorded on an Agilent 6310 ion trap mass spectrometer (ESI source, Agilent Technologies, Inc., Santa Clara, CA, USA) connected to an Agilent 1200 series HPLC with quaternary pump, vacuum degasser, diode-array detector, and autosampler.

[^{11}C]CO₂ (1.2 Ci) was obtained *via* the ^{14}N (*p*, α) ^{11}C reaction on nitrogen with 2.5% oxygen, with 11 MeV protons (Siemens Eclipse cyclotron, Siemens Healthcare GmbH, Erlangen,

Germany), and trapped on molecular sieves in a TRACERlab FX-MeI synthesizer (General Electric, GE Healthcare, Boston, MA, USA). [^{11}C]CH₄ was obtained by the reduction of [^{11}C]CO₂ in the presence of Ni/hydrogen at 350 °C and recirculated through an oven containing I₂ to produce [^{11}C]CH₃I *via* a radical reaction.

All animal studies were carried out at Massachusetts General Hospital (MGH, PHS Assurance of Compliance No. A3596-01). The Subcommittee on Research Animal Care (SRAC) serves as the Institutional Animal Care and Use Committee (IACUC) for the Massachusetts General Hospital. SRAC reviewed and approved all procedures detailed in this paper.

Micro PET-CT imaging was performed in anesthetized (isoflurane) mice (BALB/c) to minimize discomfort. Highly trained animal technicians monitored animal safety throughout all procedures, and veterinary staff were responsible for daily care. All mice were socially housed in cages appropriate for the physical and behavioral health of the individual animal and were given unlimited access to food and water, with additional nutritional supplements provided as prescribed by the attending veterinary staff.

4.2. Chemical synthesis

4.2.1. General procedure for the preparation of intermediates **9** and **10**

6-Hydroxy-2-(4-methoxyphenyl)pyridazin-3(2H)-one (9). To a mixture of (4-methoxyphenyl)hydrazine hydrochloride (7, 55 mmol) and maleic anhydride (50 mmol) in H₂O (400 mL), concentrated hydrochloric acid solution (40 mL) was added slowly with stirring. The mixture was heated at 120 °C for 8 h. The progress of the reaction was monitored by TLC. After cooling to room temperature and filtrating, the resulting solid was washed with ice-water and dissolved in a saturated sodium bicarbonate solution. After another filtration, the resulting filtrate was neutralized with 1 mol/L hydrochloric acid and formed a precipitate. The precipitate was then filtered and washed with water to yield 6-hydroxy-2-(4-methoxyphenyl)pyridazin-3(2H)-one, **9**, as a white solid (7.22 g, 66.2%). ^1H NMR (500 MHz, chloroform-*d*) δ 7.49 (d, *J* = 8.7 Hz, 2H), 7.10–7.02 (m, 2H), 7.00–6.94 (m, 2H), 3.84 (s, 3H). A signal for the OH-proton is not visible. LC–MS Calcd. for C₁₁H₁₀N₂O₃ expected [M+H]⁺: 219.1; Found [M+H]⁺: 219.1.

2-(3,4-Dichlorophenyl)-6-hydroxypyridazin-3(2H)-one (10). The procedure described for the synthesis of **9** was applied to the initial compound **8** (55 mmol), maleic anhydride (50 mmol), and H₂O (400 mL) with concentrated HCl solution (40 mL) to afford 2-(3,4-dichlorophenyl)-6-hydroxypyridazin-3(2H)-one, **10** as a white solid (9.01 g, 70.1%). ^1H NMR (500 MHz, chloroform-*d*) δ 7.89 (d, *J* = 2.3 Hz, 1H), 7.65 (dd, *J* = 8.7, 2.5 Hz, 1H), 7.52 (d, *J* = 8.8 Hz, 1H), 7.01 (s, 2H). A signal for the OH-proton is not visible. LC–MS Calcd. for C₁₀H₆Cl₂N₂O₂ expected [M+H]⁺: 258.1; Found [M+H]⁺: 258.1.

4.2.2. General procedure for the preparation of intermediates **11** and **12**

6-(3-Bromopropoxy)-2-(4-methoxyphenyl)pyridazin-3(2H)-one (11). To a solution of **9** (10 mmol) and 1,3-dibromopropane (20 mmol) in acetone (100 mL), potassium carbonate (20 mmol) was added and the mixture was refluxed for 4 h. The progress of the reaction was monitored by TLC. After cooled to room temperature, the mixture was filtered and the solvent was evaporated under reduced pressure. The crude product was purified by means

of flash chromatography (hexane/ethyl acetate = 50/1) to yield 6-(3-bromopropoxy)-2-(4-methoxyphenyl)pyridazin-3(2*H*)-one, **11**, as a pale-yellow oil (1.89 g, 55.6%). ¹H NMR (500 MHz, chloroform-*d*) δ 7.57 (d, *J* = 8.8 Hz, 2H), 7.06–7.01 (m, 2H), 7.00–6.95 (m, 2H), 4.31 (t, *J* = 5.9 Hz, 2H), 3.84 (s, 3H), 3.55 (t, *J* = 6.4 Hz, 2H), 2.30 (p, *J* = 6.2 Hz, 2H). ¹³C NMR (126 MHz, chloroform-*d*) δ 158.89, 152.50, 134.68, 134.08, 126.56, 126.36, 113.96, 64.80, 55.62, 31.75, 29.61. LC–MS Calcd. for C₁₄H₁₅BrN₂O₃ expected [M+H]⁺: 340.2; Found [M+H]⁺: 340.1.

6-(3-Bromopropoxy)-2-(3,4-dichlorophenyl)pyridazin-3(2H)-one (12). The procedure described for the synthesis of **11** was applied to intermediate **10** (10 mmol), 1,3-dibromopropane (20 mmol), and potassium carbonate (20 mmol) in acetone (100 mL) to afford 6-(3-bromopropoxy)-2-(3,4-dichlorophenyl)pyridazin-3(2*H*)-one, **12** as a light yellow oil (1.97 g, 52.0%). ¹H NMR (500 MHz, chloroform-*d*) δ 7.88 (d, *J* = 2.3 Hz, 1H), 7.64 (dd, *J* = 8.7, 2.5 Hz, 1H), 7.51 (d, *J* = 8.8 Hz, 1H), 7.00 (s, 2H), 4.33 (t, *J* = 5.9 Hz, 2H), 3.56 (t, *J* = 6.5 Hz, 2H), 2.32 (p, *J* = 6.2 Hz, 2H). ¹³C NMR (126 MHz, chloroform-*d*) δ 158.55, 152.77, 140.63, 134.34, 132.58, 131.48, 130.23, 127.23, 126.70, 124.09, 65.01, 31.62, 29.47. LC–MS Calcd. for C₁₃H₁₁BrCl₂N₂O₂ expected [M+H]⁺: 379.1; Found [M+H]⁺: 379.1.

4.2.3. General procedure for the preparation of compounds **13** to **15**

2-(4-Methoxyphenyl)-6-(3-(piperidin-1-yl)propoxy)pyridazin-3(2H)-one (13). A mixture of intermediate **11** (5 mmol) and piperidine (5.5 mmol) in acetonitrile (50 mL) and cesium carbonate (10 mmol) was heated and refluxed for 2 h. After filtering, the resulting filtrate was evaporated to dryness under reduced pressure. The residue was suspended in water (50 mL) and extracted with dichloromethane (3 × 25 mL). The combined organic layers were dried with anhydrous magnesium sulfate, the filtrate was evaporated under reduced pressure, and the crude product was purified by means of flash chromatography (CH₂Cl₂/CH₃OH = 10/1) to yield 2-(4-methoxyphenyl)-6-(3-(piperidin-1-yl)propoxy)pyridazin-3(2*H*)-one, **13**, as a yellow oil (1.46 g, 84.8%). ¹H NMR (500 MHz, chloroform-*d*) δ 7.56 (d, *J* = 8.7 Hz, 2H), 7.03–6.93 (m, 4H), 4.19 (t, *J* = 6.4 Hz, 2H), 3.84 (s, 3H), 2.53–2.30 (m, 6H), 1.96 (p, *J* = 6.7 Hz, 2H), 1.60 (p, *J* = 5.6 Hz, 4H), 1.51–1.40 (m, 2H). ¹³C NMR (126 MHz, chloroform-*d*) δ 158.91, 158.81, 152.79, 134.81, 133.89, 126.79, 126.38, 113.93, 65.86, 55.98, 55.61, 54.67, 26.23, 25.90, 24.40. LC–MS Calcd. for C₁₉H₂₅N₃O₃ expected [M+H]⁺: 344.2; Found [M+H]⁺: 344.2, HR-MS Calcd. for C₁₉H₂₅N₃O₃ expected [M+H]⁺: 344.1964; Found [M+H]⁺: 344.1969.

tert-Butyl 4-(3-((1-(3,4-dichlorophenyl)-6-oxo-1,6-dihydropyridazin-3-yl)oxy)propyl)piperazine-1-carboxylate (14). The procedure described for the synthesis of **13** was applied to intermediate **12** (5 mmol), *tert*-butyl piperazine-1-carboxylate (5.5 mmol), and cesium carbonate (10 mmol) in acetonitrile (50 mL) to afford 4-(3-((1-(3,4-dichlorophenyl)-6-oxo-1,6-dihydropyridazin-3-yl)oxy)propyl)piperazine-1-carboxylate, **14** as a light yellow oil (1.78 g, 73.5%). ¹H NMR (500 MHz, chloroform-*d*) δ 7.87 (d, *J* = 2.5 Hz, 1H), 7.64 (dd, *J* = 8.8, 2.4 Hz, 1H), 7.51 (d, *J* = 8.8 Hz, 1H), 6.99 (s, 2H), 4.23 (t, *J* = 6.4 Hz, 2H), 3.44–3.30 (m, 4H), 2.50 (t, *J* = 7.3 Hz, 2H), 2.45–2.34 (m, 4H), 1.96 (p, *J* = 6.7 Hz, 2H), 1.46 (s, 9H). ¹³C NMR (126 MHz, chloroform-*d*) δ 158.59, 153.05, 140.74, 134.13, 132.53, 131.38, 130.18, 127.49, 126.72, 124.13, 65.88, 55.11, 55.04, 53.18, 46.05, 26.16. LC–MS Calcd. for C₂₂H₂₈Cl₂N₄O₄ expected [M+H]⁺: 484.4; Found [M+H]⁺: 484.3.

2-(3,4-Dichlorophenyl)-6-(3-(4-methylpiperazin-1-yl)propoxy)pyridazin-3(2H)-one (15). The procedure described for the synthesis of **13** was applied to intermediate **12** (5 mmol), 1-methylpiperazine (5.5 mmol), and cesium carbonate (10 mmol) in acetonitrile (50 mL) to afford 2-(3,4-dichlorophenyl)-6-(3-(4-methylpiperazin-1-yl)propoxy)pyridazin-3(2*H*)-one, **15** as a light yellow oil (1.60 g, 80.6%). ¹H NMR (500 MHz, chloroform-*d*) δ 7.87 (d, *J* = 2.4 Hz, 1H), 7.64 (dd, *J* = 8.7, 2.4 Hz, 1H), 7.50 (d, *J* = 8.7 Hz, 1H), 6.99 (s, 2H), 4.22 (t, *J* = 6.4 Hz, 2H), 2.62–2.40 (m, 10H), 2.31 (s, 3H), 1.96 (p, *J* = 6.7 Hz, 2H). ¹³C NMR (126 MHz, chloroform-*d*) δ 158.57, 154.80, 153.03, 140.72, 134.16, 132.53, 131.39, 130.18, 127.45, 126.70, 124.11, 79.76, 65.76, 55.11, 55.04, 53.10, 28.51, 26.07. LC–MS Calcd. for C₁₈H₂₂Cl₂N₄O₂ expected [M+H]⁺: 396.1; Found [M+H]⁺: 397.2, HR-MS Calcd. for C₁₈H₂₂Cl₂N₄O₂ expected [M+H]⁺: 397.1193; Found [M+H]⁺: 397.1190.

2-(4-Hydroxyphenyl)-6-(3-(piperidin-1-yl)propoxy)pyridazin-3(2H)-one (16, precursor P1) Under N₂, a solution of **13** (1 mmol) in dichloromethane (14 mL) was kept in an acetone-dry ice bath at –78 °C. 6 mL of Boron tribromide solution (1.0 mol/L in dichloromethane) was added carefully to the stirring solution and kept at –78 °C for 2 h. As the solution of boron tribromide was added, a pale yellow precipitate formed. The reaction mixture was gradually warmed to room temperature and kept stirring overnight. The reaction mixture was then hydrolyzed by careful shaking with 40 mL of H₂O, thus precipitating a white solid, which was dissolved by the addition of 30 mL of dichloromethane. The organic layer was separated and extracted with 20 mL of 2 mol/L sodium hydroxide; the alkaline extract was neutralized with dilute hydrochloric acid and extracted with dichloromethane (3 × 10 mL). The combined organic layers were dried with anhydrous magnesium sulfate, the filtrate was evaporated under reduced pressure, and the crude product was purified by means of flash chromatography (CH₂Cl₂/CH₃OH = 10/1) to yield 2-(4-hydroxyphenyl)-6-(3-(piperidin-1-yl)propoxy)pyridazin-3(2*H*)-one (**16**, precursor **P1**) as a pale yellow oil (0.142 g, 43.2%). ¹H NMR (500 MHz, chloroform-*d*) δ 7.32 (d, *J* = 8.5 Hz, 2H), 7.00–6.91 (m, 2H), 6.84–6.73 (m, 2H), 4.17 (t, *J* = 6.2 Hz, 2H), 3.00–2.44 (m, 6H), 2.08 (t, *J* = 7.5 Hz, 2H), 1.82–1.66 (m, 4H), 1.59–1.41 (m, 2H). A weak signal for the Ar–OH–proton is in δ 8.04, hardly visible. ¹³C NMR (126 MHz, chloroform-*d*) δ 159.17, 156.92, 152.77, 133.59, 133.39, 126.89, 126.53, 115.74, 65.32, 55.57, 54.22, 25.02, 24.61, 23.52. LC–MS Calcd. for C₁₈H₂₃N₃O₃ expected [M+H]⁺: 330.2; Found [M+H]⁺: 330.2, HR-MS Calcd. for C₁₈H₂₃N₃O₃ expected [M+H]⁺: 330.1812; Found [M+H]⁺: 330.1813.

2-(3,4-Dichlorophenyl)-6-(3-(piperazin-1-yl)propoxy)pyridazin-3(2H)-one (17, precursor P2) Under N₂, a solution of **14** (1 mmol) in dichloromethane (18 mL) was kept in an ice bath at 0 °C. 2 mL of hydrogen chloride solution (1.0 mol/L in diethyl ether) was added to the stirring solution. As the solution of hydrogen chloride was added, a pale yellow precipitate was formed. The reaction mixture was gradually warmed to room temperature and kept stirring overnight. After that, the reaction mixture was neutralized by 30 mL of saturated sodium bicarbonate solution and extracted with dichloromethane (3 × 10 mL). The combined organic layers were dried with anhydrous magnesium sulfate, the filtrate was evaporated under reduced pressure, and the crude product was purified by means of flash chromatography (CH₂Cl₂/CH₃OH = 10/1) to yield 2-(3,4-dichlorophenyl)-6-(3-(piperazin-1-yl)propoxy)pyridazin-3(2*H*)-one (**17**, precursor **P2**) as a yellow oil (0.353 g,

92.1%). 1H NMR (500 MHz, chloroform-*d*) δ 7.86 (d, $J=2.4$ Hz, 1H), 7.63 (dd, $J=8.8, 2.4$ Hz, 1H), 7.51 (d, $J=8.7$ Hz, 1H), 7.03–6.95 (m, 2H), 4.22 (t, $J=6.4$ Hz, 2H), 3.25–3.16 (m, 2H), 3.09–2.40 (m, 9H), 2.09–1.89 (m, 2H). ^{13}C NMR (126 MHz, chloroform-*d*) δ 158.54, 152.93, 134.27, 134.19, 130.24, 130.20, 127.42, 127.34, 126.72, 124.14, 65.31, 54.58, 50.08, 43.80, 25.88. LC–MS Calcd. for $C_{17}H_{20}Cl_2N_4O_2$ expected $[M+H]^+$: 383.1; Found $[M+H]^+$: 383.1, HR-MS Calcd. for $C_{17}H_{20}Cl_2N_4O_2$ expected $[M+H]^+$: 383.1036; Found $[M+H]^+$: 383.1032.

4.3. Radiosynthesis

$[^{11}C]HCC0923$. $[^{11}C]$ methyl iodide ($[^{11}C]CH_3I$) was trapped in a TRACERlab FX-M synthesizer reactor (General Electric) preloaded with a solution of precursor **P1** in anhydrous DMF (2.0 mg/mL, 0.3 mL) and NaOH (8 mg). The solution was stirred at 120 °C for 3 min, and 0.1% trifluoroacetic acid (TFA) in water (1.2 mL) was added. The reaction mixture was purified by reverse phase semipreparative HPLC (Agilent Eclipse XDB-C18, 5 μ m, 250 mm \times 9.4 mm, flow rate=5.0 mL/min, mobile phase=0.1% TFA in water/0.1% TFA in acetonitrile, 82/18, *v/v*), and the desired fraction was collected. The final product was reformulated by loading onto a solid-phase exchange (SPE) C-18 cartridge, rinsing with H_2O (5 mL), eluting with DMSO (1 mL), and diluting with saline solution (0.9%, 9 mL).

The average time required for the synthesis from end of cyclotron bombardment to end of synthesis was approximate 40–50 min. The average radiochemical yield was 6%–15% (non-decay corrected to trapped $[^{11}C]CH_3I$). Chemical and radiochemical purities were $\geq 95\%$ with a specific activity 1.29 ± 0.2 Ci/ μ mol (EOB).

$[^{11}C]HCC0929$. $[^{11}C]$ methyl iodide ($[^{11}C]CH_3I$) was trapped in a TRACERlab FX-M synthesizer reactor (General Electric) preloaded with a solution of precursor **P2** in anhydrous DMF (2.0 mg/mL, 0.3 mL) and K_2CO_3 (8 mg). The solution was stirred at 120 °C for 3 min, and 0.1 mol/L ammonium formate (AF) in water (1.2 mL) was added. The reaction mixture was purified by reverse phase semipreparative HPLC (Phenomenex Luna 5u C8(2), 250 mm \times 10 mm, 5 μ m, flow rate=5.0 mL/min, mobile phase=0.1 mol/L AF in water/acetonitrile, 65/35, *v/v*), and the desired fraction was collected. The final product was reformulated by loading onto a solid-phase exchange (SPE) C-18 cartridge, rinsing with H_2O (5 mL), eluting with EtOH (1 mL), and diluting with saline solution (0.9%, 9 mL).

The average time required for the synthesis from end of cyclotron bombardment to end of synthesis was approximate 40–50 min. The average radiochemical yield was 3%–8% (nondecay corrected to trapped $[^{11}C]CH_3I$). Chemical and radiochemical purities were $\geq 95\%$ with a specific activity 1.62 ± 0.2 Ci/ μ mol (EOB).

4.4. Molecular docking

Molecular docking into the σ_1R was performed in the manner of previous work^{13,14,35} with Glide 5.5 extra precision (XP) Maestro 11 Schrodinger software (Schrodinger, LLC, New York, NY, USA) release 2016–3⁴¹.

The 2.5 Å resolution structure of σ_1R in complex with PD 144418 (PDB 5KH1) was used for docking, compared with the *ex vivo* binding affinity⁴². Because the structure has three protomers in the asymmetric unit, only chain C was used for

docking studies. Lipids, ions, and waters were removed before protein preparation, thus leaving only the protein and ligand. Hydrogen atoms were added, and the protein was further refined by assignment of hydrogen bonds and minimization of energy for the OPLS3 force field. The grid used for docking was centered on the location of the co-crystallized ligand PD 144418, and was 20 Å in the *x*, *y*, and *z* dimensions. Poses were ranked according to glide score and inspected visually. Only poses in which the ligand's basic amine made an electrostatic interaction with E172 were considered plausible, as this has been observed in all five existing σ_1R crystal structures currently available^{13,14}.

4.5. Mice PET-CT acquisition and post processing

Male Balb/c mice were tested in groups, each group contained 4 mice, anesthetized with inhalational isoflurane (Patterson Vet Supply, Inc., Greeley, CO, USA) at 2% in a carrier of 2 L/min medial oxygen, and maintained at 1% isoflurane for the duration of the scan.

The mice were arranged side-by-side in two layers in a Triumph Trimodality PET/CT/SPECT scanner (Gamma Medica, Northridge, CA, USA). Mice were injected standard references or vehicle *via* a lateral tail vein catheterization at the start of PET acquisition. Dynamic PET acquisition lasted for 60 min followed by computed tomography (CT) for anatomic coregistration. PET data were reconstructed using a 3D-MLEM method resulting in a full width at half-maximum resolution of 1 mm. Reconstructed images were exported from the scanner in DICOM format along with an anatomic CT for rodent studies. These files were imported and analyzed using AMIDE (a medical imaging data examiner) software (an open-source software, Los Angeles, CA, USA)⁴³ and PMOD (PMOD4.003, PMOD Technologies Ltd., Zurich, Switzerland).

4.6. Mice PET-CT image analysis

Volumes of interest (VOIs) were generated manually in forms of spheres under the guide of high-resolution CT structural images and summed PET data in mice brain regions, with a radius no less than 1 mm to minimize partial volume effects. Time-activity curves (TACs) were exported as decay-corrected activity per unit volume. The TACs were expressed as percent injected dose per unit volume for analysis.

Acknowledgments

This work was supported by a pilot funding from the Athinoula A. Martinos Center for Biomedical Imaging at the Massachusetts General Hospital (Changning Wang, USA), National Natural Science Foundation of China (Grant No.81602946, Yu Lan) and Natural Science Foundation of Hubei Province of China (Grant No. 2016CFB258, Yu Lan). The authors are grateful to Prof. Andrew C. Kruse in Department of Biological Chemistry and Molecular Pharmacology, Harvard Medical School for the constructive discussion and enthusiastic help in molecular docking, the Athinoula A. Martinos Center Radiopharmacy Lab staff for assistant in radiochemistry and Prof. Xudong Cao in Xuzhou Medical School for the discussion in chemistry and structure identification.

Appendix A. Supporting information

Supporting data to this article can be found online at <https://doi.org/10.1016/j.apsb.2019.07.002>.

References

- Martin WR, Eades CG, Thompson JA, Huppler RE, Gilbert PE. The effects of morphine- and nalorphine- like drugs in the nondependent and morphine-dependent chronic spinal dog. *J Pharmacol Exp Ther* 1976;**197**:517–32.
- Zukin SR, Brady KT, Slifer BL, Balster RL. Behavioral and biochemical stereoselectivity of sigma opiate/PCP receptors. *Brain Res* 1984;**294**:174–7.
- Hellewell SB, Bowen WD. A sigma-like binding site in rat pheochromocytoma (PC12) cells: decreased affinity for (+)-benzomorphans and lower molecular weight suggest a different sigma receptor form from that of Guinea pig brain. *Brain Res* 1990;**527**:244–53.
- Su TP, Su TC, Nakamura Y, Tsai SY. The sigma-1 receptor as a pluripotent modulator in living systems. *Trends Pharmacol Sci* 2016;**37**:262–78.
- Hanner M, Moebius FF, Flandorfer A, Knaus HG, Striessnig J, Kempner E, et al. Purification, molecular cloning, and expression of the mammalian sigma1-binding site. *Proc Natl Acad Sci U S A* 1996;**93**:8072–7.
- Alon A, Schmidt HR, Wood MD, Sahn JJ, Martin SF, Kruse AC. Identification of the gene that codes for the σ_2 receptor. *Proc Natl Acad Sci U S A* 2017;**114**:7160–5.
- Pabba M. The essential roles of protein–protein interaction in sigma-1 receptor functions. *Front Cell Neurosci* 2003;**7**:50.
- Hayashi T, Su TP. Regulating ankyrin dynamics: roles of sigma-1 receptors. *Proc Natl Acad Sci U S A* 2001;**98**:491–6.
- Hayashi T, Su TP. Sigma-1 receptor chaperones at the ER–mitochondrion interface regulate Ca^{2+} signaling and cell survival. *Cell* 2007;**131**:596–610.
- Maurice T, Su TP. The pharmacology of sigma-1 receptors. *Pharmacol Ther* 2009;**124**:195–206.
- Van Waarde A, Rybczynska AA, Ramakrishnan N, Ishiwata K, Elsinga PH, Dierckx RA. Sigma receptors in oncology: therapeutic and diagnostic applications of sigma ligands. *Curr Pharmaceut Des* 2010;**16**:3519–37.
- Tesei A, Cortesi M, Zamagni A, Arienti C, Pignatta S, Zanoni M, et al. Sigma receptors as endoplasmic reticulum stress “gatekeepers” and their modulators as emerging new weapons in the fight against cancer. *Front Pharmacol* 2018;**9**:711.
- Schmidt HR, Zheng S, Gurpinar E, Koehl A, Manglik A, Kruse AC. Crystal structure of the human σ_1 receptor. *Nature* 2016;**532**:527–30.
- Schmidt HR, Betz RM, Dror RO, Kruse AC. Structural basis for σ_1 receptor ligand recognition. *Nat Struct Mol Biol* 2018;**25**:981–7.
- Brust P, Deuther-Conrad W, Lehmkühl K, Jia H, Wünsch B. Molecular imaging of σ_1 receptors *in vivo*: current status and perspectives. *Curr Med Chem* 2014;**21**:35–69.
- Weber F, Brust P, Laurini E, Priel S, Wünsch B. Fluorinated PET tracers for molecular imaging of σ_1 receptors in the central nervous system. In: Smith SB, Su TP, editors. *Sigma receptors: their role in disease and as therapeutic targets*. Cham: Springer; 2017. p. 31–48.
- Jia H, Zhang Y, Huang Y. Imaging sigma receptors in the brain: new opportunities for diagnosis of Alzheimer’s disease and therapeutic development. *Neurosci Lett* 2019;**691**:3–10.
- Toyohara J, Sakata M, Ishiwata K. PET imaging of sigma₁ receptors. In: Dierckx RA, Otte A, De Vries EF, Van Waarde A, Luitjen PG, editors. *PET and SPECT of neurobiological systems*. Berlin, Heidelberg: Springer; 2014. p. 741–63.
- Kawamura K, Ishiwata K, Tajima H, Ishii SI, Matsuno K, Homma Y, et al. *In vivo* evaluation of [¹¹C]SA4503 as a PET ligand for mapping CNS sigma₁ receptors. *Nucl Med Biol* 2000;**27**:255–61.
- Shen B, James ML, Andrews L, Lau C, Chen S, Palmer M, et al. Further validation to support clinical translation of [¹⁸F]FTC-146 for imaging sigma-1 receptors. *EJNMMI Res* 2015;**5**:49.
- Kawamura K, Tsukada H, Shiba K, Tsuji C, Harada N, Kimura Y, et al. Synthesis and evaluation of fluorine-18-labeled SA4503 as a selective sigma₁ receptor ligand for positron emission tomography. *Nucl Med Biol* 2007;**34**:571–7.
- Waterhouse RN, Collier TL. *In vivo* evaluation of [¹⁸F]1-(3-fluoropropyl)-4-(4-cyanophenoxymethyl)piperidine: a selective sigma-1 receptor radioligand for PET. *Nucl Med Biol* 1997;**24**:127–34.
- Waterhouse RN, Zhao J, Stabin MG, Ng H, Schindler-Horvat J, Chang RC, et al. Preclinical acute toxicity studies and dosimetry estimates of the novel sigma-1 receptor radiotracer, [¹⁸F]SFE. *Mol Imaging Biol* 2006;**8**:284–91.
- Waterhouse RN, Chang RC, Zhao J, Carambot PE. *In vivo* evaluation in rats of [¹⁸F]1-(2-fluoroethyl)-4-[(4-cyanophenoxy)methyl]piperidine as a potential radiotracer for PET assessment of CNS sigma-1 receptors. *Nucl Med Biol* 2006;**33**:211–5.
- James ML, Shen B, Zavaleta CL, Nielsen CH, Mesangeau C, Vuppala PK, et al. New positron emission tomography (PET) radioligand for imaging σ -1 receptors in living subjects. *J Med Chem* 2012;**55**:8272–82.
- Hjørnevik T, Cipriano PW, Shen B, Park JH, Gulaka P, Holley D, et al. Biodistribution and radiation dosimetry of ¹⁸F-FTC-146 in humans. *J Nucl Med* 2017;**58**:2004–9.
- NIH-U.S. National Library of Medicine, ClinicalTrials.gov, Identifier: NCT02753101. Available from: <https://clinicaltrials.gov/ct2/show/NCT02753101?term=FTC-146&rank=1#wrapper>.
- Cao X, Chen Y, Zhang Y, Lan Y, Zhang J, Xu X, et al. Synthesis and biological evaluation of novel σ_1 receptor ligands for treating neuropathic pain: 6-hydroxypyridazinones. *J Med Chem* 2016;**59**:2942–61.
- Lan Y, Chen Y, Cao X, Zhang J, Wang J, Xu X, et al. Synthesis and biological evaluation of novel sigma-1 receptor antagonists based on pyrimidine scaffold as agents for treating neuropathic pain. *J Med Chem* 2014;**57**:10404–23.
- McOmie JF, West DE. 3,3'-dihydroxybiphenyl. *Org Synth* 1969;**49**:50–2.
- Van De Bittner GC, Ricq EL, Hooker JM. A philosophy for CNS radiotracer design. *Acc Chem Res* 2014;**47**:3127–34.
- Weissman AD, Su TP, Hedreen JC, London ED. Sigma receptors in post-mortem human brains. *J Pharmacol Exp Ther* 1988;**247**:29–33.
- Kornhuber J, Schoppmeyer K, Bendig C, Riederer P. Characterization of [³H]pentazocine binding sites in post-mortem human frontal cortex. *J Neural Transm (Vienna)* 1996;**103**:45–53.
- Andrés A, Rosés M, Rafols C, Bosch E, Espinosa S, Segarra V, et al. Setup and validation of shake-flask procedures for the determination of partition coefficients (log *D*) from low drug amounts. *Eur J Pharm Sci* 2015;**76**:181–91.
- Linkens K, Schmidt HR, Sahn JJ, Kruse AC, Martin SF. Investigating isoindoline, tetrahydroisoquinoline, and tetrahydrobenzazepine scaffolds for their sigma receptor binding properties. *Eur J Med Chem* 2018;**151**:557–67.
- Wang C, Schroeder FA, Hooker JM. Development of new positron emission tomography radiotracer for BET imaging. *ACS Chem Neurosci* 2017;**8**:17–21.
- Wang C, Schroeder FA, Wey HY, Borra R, Wagner FF, Reis S, et al. *In vivo* imaging of histone deacetylases (HDACs) in the central nervous system and major peripheral organs. *J Med Chem* 2014;**57**:7999–8009.
- Ma Y, Hof PR, Grant SC, Blackband SJ, Bennett R, Slatest L, et al. A three-dimensional digital atlas database of the adult C57BL/6J mouse brain by magnetic resonance microscopy. *Neuroscience* 2005;**135**:1203–15.
- Mirriione MM, Schiffer WK, Fowler JS, Alexoff DL, Dewey SL, Tsirka SE. A novel approach for imaging brain-behavior relationships in mice reveals unexpected metabolic patterns during seizures

- in the absence of tissue plasminogen activator. *Neuroimage* 2007;**38**:34–42.
40. Kawamura K, Kobayashi T, Matsuno K, Ishiwata K. Different brain kinetics of two sigma₁ receptor ligands, [³H](+)-pentazocine and [¹¹C]SA4503, by P-glycoprotein modulation. *Synapse* 2003;**48**:80–6.
41. Friesner RA, Murphy RB, Repasky MP, Frye LL, Greenwood JR, Halgren TA, et al. Extra precision glide: docking and scoring incorporating a model of hydrophobic enclosure for protein-ligand complexes. *J Med Chem* 2006;**49**:6177–96.
42. Akunne HC, Whetzel SZ, Wiley JN, Corbin AE, Ninteman FW, Teclé H, et al. The pharmacology of the novel and selective sigma ligand, PD 144418. *Neuropharmacology* 1997;**36**:51–62.
43. Loening AM, Gambhir SS. AMIDE: a free software tool for multi-modality medical image analysis. *Mol Imaging* 2003;**2**:131–7.